Vulnerability assessment for earthquake-liquefaction-induced settlements of an embankment using gaussian processes

Fernando Lopez-Caballero, Christina Khalil

VULNERABILITY ASSESSMENT FOR EARTHQUAKE-LIQUEFACTION-INDUCED SETTLEMENTS OF AN EMBANKMENT USING GAUSSIAN PROCESSES

Fernando Lopez-Caballero [1], Not a Member, ASCE

Christina Khalil, [2], Associate Member, ASCE

ABSTRACT

The major cause of earthquake damage to an embankment is the liquefaction of the soil foundation that induces ground level deformations. The aim of this paper is to assess numerically the effect of the liquefaction-induced settlement of the soil foundation on an levee due to real earthquakes. The seismic vulnerability is evaluated in terms of analytical fragility curves constructed on the basis of non-linear dynamic Finite Elements (FE) analysis. However, FE analysis can be expensive due to very large number of simulations needed for an accurate assessment of the system failure behaviour. This problem is addressed by building a Gaussian Process (GP) emulator to represent the output of the expensive FE model. A comparison with the FE reference results suggests that the proposed GP model works well and can be successfully used as a predictive tool to compute the induced damage on the levee. Findings also illustrate clearly the importance and the advantages of an adequate definition of the input parameters to built the GP model.

Keywords: Liquefaction, Damage levels, Gaussian processes, Fragility functions, Performance-based methodology.

INTRODUCTION

[1]Ph.D., Associate Professor, MSS-Mat CNRS UMR 8579, CentraleSupélec Paris-Saclay University, 3 Rue Joliot-Curie, 91190 Gif-Sur-Yvette, France. E-mail: fernando.lopez-caballero@centralesupelec.fr

[2]M.Sc., graduate, MSS-Mat CNRS UMR 8579, CentraleSupélec Paris-Saclay University, 3 Rue Joliot-Curie, 91190 Gif-Sur-Yvette, France. E-mail: christina.khalil@icloud.com

Earthquakes are the most natural phenomenon that cause damage to the soil and to the structures, in addition to other losses such as human and economic. Liquefaction phenomenon is considered as one of the most devastating and complex behaviours that affect the soil due to earthquake loading. It was observed that geotechnical structures, such as river dikes, highway embankments, and earth dams, founded on saturated loose sandy ground have been frequently damaged during past major earthquakes (Matsuo 1996; Ozutsumi et al. 2002; Unjoh et al. 2012; Okamura et al. 2013). According to the state of the art in the assessment of earthquake-induced soil liquefaction performed by the National Academies of Sciences, Engineering, and Medicine (2016), it is necessary *to refine, develop, and implement performance-based approaches to evaluating liquefaction, including triggering, the geotechnical consequence of triggering, structural damage, and economic loss models to facilitate performance-based evaluation and design.* The Pacific Earthquake Engineering Research Center (PEER)'s performance-based earthquake engineering methodology deals with four stages: the hazard analysis in which an intensity measure (IM) parameter is identified, the structural analysis in which the response to the earthquake is represented by the engineering demand parameter (EDP), the damage analysis in which the probability of failure is quantified and the final stage is the loss analysis which requires the estimation of the decision based on the cost and maintenance of the project (Porter 2003; Baker and Cornell 2008a). The present work would be dealing with two stages of this methodology: the structural and the damage analyses. The dynamic structural analysis requires a deterministic approach to calculate the used parameters of the study. As the final objective is to evaluate expected losses, it is necessary to perform a large number of non-linear calculations, providing sufficient details about the damage state and with an acceptable computational cost. Previous works have used such approach to study the apparition of soil liquefaction and their effects on the response of the structures or dams (Koutsourelakis et al. 2002; Juang et al. 2005; Popescu et al. 2006; Lopez-Caballero and Modaressi-Farahmand-Razavi 2010).

The aim of this work is to assess numerically the effect of soil liquefaction-induced failure

to a levee due to real earthquakes. A deterministic study to quantify a failure way of a levee (crest settlement) and a probabilistic study to find the probability of exceedance of a certain level of performance, took place. As a first approach, only the aspects concerning the uncertainties in the seismic ground motion are addressed. Fragility functions were drawn for this purpose. The Finite Element (FE) calculations were performed using the GEFDyn code and the numerical model was inspired from the one proposed by Rapti et al. (2017). Consequently, a database including a great number of ground motions is required to provide enough information to estimate in a reliable way the parameters defining the fragility curves (Luco and Cornell 2007; Saez et al. 2011).

However, due to the high computational cost to perform the numerous non-linear dynamic calculations, it is no feasible to explore a large design space using the complex proposed Finite Element model (FEM). In this context, fast-running models, also called surrogate models could be implemented by means of input-output data sets to approximate the response of the original FEM. Several kinds of surrogate models (e.g. Linear regression, Neural networks, Chaos polynomials, support vector machines among others) have been implemented to assess the damage of non linear structures or networks under earthquake loading (Bucher and Most 2008; Cardoso et al. 2008; Seo et al. 2012; Ghosh et al. 2013; Gidaris et al. 2015; Ferrario et al. 2017; Stern et al. 2017). Hence, in this work a Gaussian Process model (GPM) was used as a surrogate model for the levee-foundation system, so as to reduce the computation time associated keeping an accurate prediction (Sacks et al. 1989; Toal et al. 2008). The GPM was built using input model parameters that are relevant to represent system response of the inelastic transient FE analysis. Once the GPM was trained and validated, it is applied to quantify the effect of soil liquefaction-induced failure on a levee subject to a large variety of earthquake events. In particular, the maximal induced crest settlement is computed and the corresponding fragility curves for a given damage threshold are estimated. Although Gaussian process emulators have been used in other disciplines, there is no knowledge of it having been implemented in the framework of performance-based approaches to evaluating

liquefaction induced damage of dams or embankments.

In the next section, a brief description of a construction of Gaussian process model is given. In the third section, a synthetic description of the Finite Element model used to simulate the levee is provided. Next, the main results of the analysis with the FEM are presented. In the the fifth section, the choice of the input parameters and the validation of the GPM in terms of its capability of prediction are shown. In the last section, intensive simulations are performed with the GPM in order to estimate the fragility curves for a given levee damage threshold. Finally, conclusions summarizing the obtained results and future developments of this work are provided.

GAUSSIAN PROCESS EMULATOR

A meta-model or surrogate model is an analytical function used to provide rapid approximations of more expensive models (e.g. an analytical model or a finite element numerical model). In the Gaussian process (GP), the responses and input values are combined statistically to create functional relationships in a non-intrusive approach (i.e. the original model is considered as a black box). One of the advantages of Gaussian processes is that they are flexible enough to represent a wide variety of complex models using a limited number of parameters. In contrast to other kind of meta-models (e.g. Linear regression, Neural networks, Chaos polynomials among others), GP provides a function that does not depend on the probabilistic model for the input data.

Let us consider a non-linear computer model response, that could be represented by a multivariate function $\mathbf{y} = f(\mathbf{x})$; where $\mathbf{x}$ is a d-dimensional vector describing the input parameters of the model and $\mathbf{y}$ is a vector of n observed outputs. Usually, $f(\mathbf{x})$ is deterministic whenever the same input ($\mathbf{x}$) results in the same output ($\mathbf{y}$). It is also assumed that evaluation of $f(\mathbf{x})$ is computationally expensive, thus, only limited function evaluations $\mathbf{y_1} = f(\mathbf{x_1}), \ldots, \mathbf{y_n} = f(\mathbf{x_n})$ are available. These evaluations are called experimental design (ED) and they are used as a database for training or learning the meta-model (i.e. the learning database LDB). The purpose of the meta-model is therefore to predict the response

($\mathbf{y} = f(\mathbf{x}^*)$) for a new data set where only the input $\mathbf{x}^*$ are known (i.e. the test database, TDB) (Sacks et al. 1989; Rasmussen and Williams 2006; DiazDelaO et al. 2013; Dubourg et al. 2013; Strong and Oakley 2014). Hence, it is possible to obtain a statistical approximation to the output of a numerical model after evaluating a small number n of design points if $f(\mathbf{x})$ is modelled as a Gaussian process (GP). A GP is a collection of random variables, which have a joint multivariate Gaussian distribution. The GP model will be separated in mean and covariance functions :

$$f(\mathbf{x}) \quad = \quad \mathbf{h}(\mathbf{x})^T \boldsymbol{\beta} + Z(\mathbf{x}) \tag{1}$$

where $\mathbf{h}(\mathbf{x})^T \boldsymbol{\beta}$ is the mean function (usually modelled as a generalized linear model and sometimes times assumed to be zero), $\mathbf{h}(\mathbf{x})$ is a vector of known functions and $\boldsymbol{\beta}$ is a vector of unknown coefficients. The function $Z(\mathbf{.})$ is a Gaussian process with mean zero and covariance function $\mathsf{Cov}(Z(\mathbf{x}), Z(\mathbf{x}')|\sigma^2, \theta)$ between output points corresponding to input points $\mathbf{x}$ and $\mathbf{x}'$:

$$\mathsf{Cov}(Z(\mathbf{x}), Z(\mathbf{x}')|\sigma^2, \theta) \quad = \quad \sigma^2 \cdot c_\theta(\mathbf{x}, \mathbf{x}') \tag{2}$$

where σ^2 is the variance of Z, θ the range parameter and $c_\theta(\ ,\ )$ its correlation function. The GP assumes that the correlation between $Z(\mathbf{x})$ and $Z(\mathbf{x}')$ is a function of the "*distance*" between $\mathbf{x}$ and $\mathbf{x}'$. The covariance can be any function having the property of generating a positive definite covariance matrix (Rasmussen and Williams 2006; Iooss et al. 2010). A wide variety of covariance functions could be used in the Gaussian process framework, thus, in this work three common correlation functions were used, namely, exponential (equation

3), Matérn (3/2) (equation 4) and γ-exponential (equation 5).

$$c_\theta(\mathbf{x}, \mathbf{x}') = \exp\left\{-\sum_{i=1}^{d} \frac{\mid x_i - x_i' \mid}{\theta_i}\right\} \tag{3}$$

$$c_\theta(\mathbf{x}, \mathbf{x}') = \left(1 + \frac{\sqrt{3}}{\theta}\|\mathbf{x} - \mathbf{x}'\|\right) \exp\left(-\frac{\sqrt{3}}{\theta}\|\mathbf{x} - \mathbf{x}'\|\right) \tag{4}$$

$$c_\theta(\mathbf{x}, \mathbf{x}') = \exp\left\{-\sum_{i=1}^{d} \left(\frac{x_i - x_i'}{\theta_i}\right)^\gamma\right\} \tag{5}$$

for $\mathbf{x} = (x_1, \ldots, x_d)$. Note that equation 4 is parametrized as in Genton (2001). The hyper-parameters involved in each covariance function are estimated by likelihood maximization. Finally, the predictor and the variance of the GP for the new input $\mathbf{x}^*$ are estimated as follows:

$$\mathbf{E}\left(f(\mathbf{x}^*)\right) = \mathbf{h}(\mathbf{x}^*)^T\boldsymbol{\beta} + \mathbf{k}(\mathbf{x}^*)^T\boldsymbol{\Sigma}^{-1}(f(\mathbf{x}) - \mathbf{h}(\mathbf{x})^T\boldsymbol{\beta}) \tag{6}$$

$$\mathrm{Var}\left(f(\mathbf{x}^*)\right) = \sigma^2 - \mathbf{k}(\mathbf{x}^*)^T\boldsymbol{\Sigma}^{-1}\mathbf{k}(\mathbf{x}^*) \tag{7}$$

$$\mathbf{k}(\mathbf{x}^*) = \sigma^2[c_\theta(\mathbf{x_1}, \mathbf{x}^*), \ldots, c_\theta(\mathbf{x_n}, \mathbf{x}^*)]^T \tag{8}$$

$$\boldsymbol{\Sigma} = \sigma^2\left(c_\theta(\mathbf{x_i}, \mathbf{x_j})_{i=1\ldots n\,, j=1\ldots n}\right) \tag{9}$$

where $\boldsymbol{\Sigma}$ is the covariance matrix. Refer to Sacks et al. (1989), Rasmussen and Williams (2006) or Iooss et al. (2010) among others for further details about the GP meta-model.

SELECTED LEVEE CASE STUDY

The geometry of the model, as shown in Figure 1(a), consists of an embankment of 9m high composed of dry dense sand. The soil foundation is composed of a liquefiable loose-to-medium sand (LMS) of 4m at the top of a saturated dense sand of 6m. The bedrock at the bottom of the dense sand has a shear wave velocity (V_s) equal to 1000m/s and a mass density (ρ_{bd}) of 2000kg/m^3. The water table is situated at 1m below the base of the embankment and it was kept dry. The levee's inclination is a slope of 1:3 (vertical: horizontal). The geometry used in the FEM was inspired from the one proposed by Rapti et al. (2017).

All computations were conducted with GEFD*yn* FE code (Aubry et al. 1986; Aubry and Modaressi 1996). The elastoplastic multi-mechanism model briefly described below is used to represent the soil behaviour (Figure 1(a)). For the bedrock representing a half-space, an isotropic linear elastic behaviour was assumed. The model length is 194m.

A 2D coupled dynamic approach derived from the $\underline{u}-p_w$ version of the Biot's generalized consolidation theory (Zienkiewicz and Shiomi 1984) was adopted for the soil. The so-called $\underline{u}-p_w$ formulation, consists of neglecting fluid acceleration terms and convective terms of this acceleration so that the unknown variables remain the displacement of the solid $\underline{u}$ and the pressure of the water p_w. The saturated soil was modelled using quadrilateral isoparametric elements with eight nodes for both solid displacements and fluid pressures. The size of elements is 0.5m×0.5m. It was chosen in order to have 8 to 10 elements per wavelength which are sufficient to prevent numerical dispersion. A plane-strain condition was assumed in the finite element model. In the analysis, only vertically incident shear waves are introduced into the domain and as the response of an infinite semi-space is modelled, equivalent boundaries have been imposed on the nodes of lateral boundaries (i.e. the normal stress on these boundaries remains constant and the displacements of nodes at the same depth in two opposite lateral boundaries are the same in all directions). The model is 194m wide so as to ensure that the effect of the boundaries on the model response can be neglected and also to satisfy the free field condition at the lateral boundaries. For the half-space bedrock's boundary condition, paraxial elements simulating "*deformable unbounded elastic bedrock*" have been used (Modaressi and Benzenati 1994). The incident waves, defined at the outcropping bedrock are introduced into the base of the model after deconvolution.

The elastoplastic multi-mechanism model developed at *Ecole Centrale Paris* (ECP) (Aubry et al. 1982) is used to represent the soil behaviour. This model can take into account the soil behaviour in a large range of deformations. The model is written in terms of effective stress. The representation of all irreversible phenomena is made by four coupled elementary plastic mechanisms: three plane-strain deviatoric plastic deformation mechanisms

in three orthogonal planes and an isotropic one. The model uses a Coulomb-type failure criterion and the critical state concept. The evolution of hardening is based on the plastic strain (deviatoric and volumetric strain for the deviatoric mechanisms and volumetric strain for the isotropic one). To take into account the cyclic behaviour a kinematical hardening based on the state variables at the last load reversal is used. The soil behaviour is decomposed into pseudo-elastic, hysteretic and mobilized domains. Refer to Aubry et al. (1982), Lopez-Caballero and Modaressi-Farahmand-Razavi (2008) among others for further details about the ECP model. The obtained curves of cyclic stress ratio ($SR = \sigma_{v-cyc}/(2 \cdot p'_o)$, with σ_{v-cyc} the cyclic vertical stress applied in the cyclic loading) as a function of the number of loading cycles to produce liquefaction (N) and $G/G_{max} - \gamma$ curves are given in Figure 1(a). As qualitative comparison, the modelled test results are compared with the experimentally obtained curves given by Byrne et al. (2004) for Nevada sand at different densities (i.e. D_r = 40% and 60%) and with the reference curves given by Seed and Idriss (1971).

Input earthquake motion

The selection of input motions for geotechnical earthquake engineering problems is important as it is strongly related to the non-linear dynamic analyses. So as to obtain analytical fragility curves, it is necessary to analyse the embankment response to a wide range of ground motions. In addition, when dealing with surrogate models, it is required to have a representative set of data to train, to validate and to test the proposed meta-model. A total of 540 unscaled records were chosen from the Pacific Earthquake Engineering Research Center (PEER) database (Ancheta et al. 2013), the Center for Engineering Strong Motion Data and the Kiban Kyoshin strong-motion network (KIK-NET) (Aoi et al. 2001). The events range between 5.2 and 7.6 in magnitude and the recordings have site-to-source distances from 15 to 50km and concern dense-to-firm soil conditions (i.e. 360m/s $< V_{s\ 30m} <$ 800m/s). All input signals have a baseline correction, a sampling time (Δt) equal to 0.005s and they are filtered using a *non-causal* 4th-order Butterworth bandpass filter (i.e. Zero-phase digital filtering), between 0.1-25Hz.

The database was split as follows : 95 signals concern the learning database (LDB), 50 ground-motions are used for the validation set (VDB) and the test database (TDB) is composed of 395 unscaled records. The statistics on some input earthquake characteristics obtained for each database are summarized in Table 1. These earthquake characteristics are maximal outcropping acceleration ($a_{max\,out}$), Arias intensity (I_A), mean period (T_m), peak ground velocity (PGV), period of equivalent harmonic wave ($T_{V/A} = \alpha \cdot PGV/a_{max\,out}$, with α=4.89) and significant duration from 5% to 95% Arias intensity (D_{5-95}).

RESULTS WITH THE LEARNING DATABASE SET (LDB)

For embankments placed in seismic zones, it has been shown that the widespread damage to such embankments occurred mainly due to the liquefaction of foundation soil, resulting in excessive settlements, lateral spreading and slope instability (Sharp and Adalier 2006; Oka et al. 2012; Okamura et al. 2013). Thus, in this study, the crest settlement is chosen to be the mode of failure because it is a quantifiable measurement. Figure 1(b) shows a zoomed view of the typical response of vertical displacement contours in the levee after the earthquake loading. The computed deformed shape is characterized by a crest settlement due to soil liquefaction in the foundation and associated with lateral spread in foundation soil. In addition, Figure 1(c) shows a box plot of the ratio of CPU time per earthquake duration spent to perform the computations using LDB and VDB sets. It is noted that for the used FE model, CPU time varies between 1.2 and 1.7 minutes per second of earthquake duration. It means that a single FEM run for an earthquake with a typical duration of 30s, takes approximatively 35 to 55 minutes.

Even if the earthquake loading applied to the soil-levee system is very complex, it is necessary to select few strong-motion intensity parameters that can be accurately represent the levee behaviour. Swaisgood (2003) analysed a historical database on the performance of dams during earthquakes and found that the crest settlement is directly related to some input ground motion characteristics (i.e. the peak ground acceleration and magnitude). In addition, he proposes four damage levels according to the induced crest settlement. Following

Swaisgood's proposition, in this work the obtained percentage crest settlement ($\delta u_{z,rel}/H$, where $u_{z,rel}$ is the crest settlement, H is the height of the dam and the foundation which is 19m as seen in Figure 1(a)) is compared to the peak ground acceleration at the outcropping bedrock ($a_{max\,out}$). To take into account all the signals in the LDB set, the crest settlement was calculated accordingly and was drawn as function of $a_{max\,out}$ (Figure 2(a)). It is interesting to note that, as expected, the calculated crest settlement increases when the acceleration at the outcrop increases.

On the other hand, it is also noticed that two motions with very different $a_{max\,out}$ values could provide the same crest settlement ratio (i.e. damage level), which implies that not only the amplitude of a motion controls the levee response. Hence, Kawase (2011) proposes to use the equivalent predominant frequency ($1/T_{V/A}$), the maximum velocity (PGV) and acceleration of the ground motion to represent the earthquake loading. Figure 2(b) displays the variation of crest settlement ratio of the FE model as a function of $a_{max\,out}$ and $1/T_{V/A}$. It is observed that the values of increasing crest settlements of the FE models follow the lines of increasing velocity. In addition, according to Kayen and Mitchell (1997) and Koutsourelakis et al. (2002) among others, the liquefaction induced seismic settlement on structures is also well correlated with the Arias intensity value, which represents the input seismic energy.

NONLINEAR SYSTEM IDENTIFICATION USING GPM

One of the problem of calibrating or training a surrogate model (GPM) to observations from the numerical model (FEM) deals with finding input values such that the GPM outputs match the observed data as closely as possible. According to the previous section, several strong-motion intensity parameters have a great influence on the levee response, e.g. $a_{max\,out}$, $1/T_{V/A}$ and I_A among others. Thus, it means that the proposed GPM will be a multiple-input single-output one. Other aspect concerns the correlation function defining the Gaussian process itself (i.e. found the unknown hyperparameters). As recalled before, three common correlation functions will be tested in this section, equations 3 to 5. The hyperparameters for those models are estimated with the R-code packages for the Analysis of Computer

Experiments developed by Roustant et al. (2012). Once the GPM was trained with the LDB set, the possible models are validated, hence, a comparison of all responses in terms of $\delta u_{z,rel}/H$ obtained with FEM and predicted by GPM using the VDB set will be done. Further, the selected GP model is tested on a database (TDB) that is similar in structure to the database which was used for training, but was not used to built the surrogate model.

Figure 3 displays a comparison of the distribution of the GPM input parameters used as training set (LDB) and the set which is used to validate the predictions of the model on new data (VDB). It concerns three possible input parameters, namely, $1/T_{V/A}$, $a_{max\,out}$ and I_A. It is important to note the great variance of those distributions and the overlap between the training data and the validation one.

In order to assess how well the GP model has been trained (i.e. Validation phase) a comparison between the $\delta u_{z,rel}/H$ values obtained with the FEM and the mean predicted ones by the GPM using the VDB set is done (Figure 4). Thus, the relative error or discrepancy between the GPM predictions (y_i^{pred}) with the FEM computations (y_i) is calculated with the predictive squared correlation coefficient (Q^2) :

$$Q^2(y_i, y_i^{pred}) = 1 - \frac{\sum_{i=1}^{N}(y_i^{pred} - y_i)^2}{\sum_{i=1}^{N}(y_i - \mu_y)^2} \tag{10}$$

where μ_y is the mean of the N observations (i.e. FEM computations). It ranges between 0 and 1. The results of the performed parametric study are summarized in Table 2 for a size of the learning sample (N_{LDB}) equal to 95. For the sake of brevity, only the two better responses are displayed in Figure 4. It is noted that, the best fit to the FEM data is given for the case when three input parameters are used and the exponential and γ-exponential covariance functions seem to provide the best predictions. When only 2 input parameters ($1/T_{V/A}$ and $a_{max\,out}$) are used to train the GPM, the best fit is obtained with the γ-exponential covariance function.

In addition, it is well know that the choice and the size of the learning samples are key

issues on the quality of the GPM predictions. Thus, in order to study the evolution of the estimated Q^2_{VDB} criteria as a function of the size of the learning sample (N_{LDB}) the following procedure was used: For both, a fixed N_{LDB} value (ranging from 20 to 95) and for a GPM type, the 95 signals from the learning database are permuted randomly and the first N_{LDB} samples are used to construct the GPM. Then, the accuracy of the prediction of the obtained GPM is evaluated using the Q^2_{VDB} criteria. This procedure is repeated 20 times for each fixed N_{LDB} value and the obtained median value is used to define the accuracy of the GPM. As example, Figure 5 displays the boxplots of the obtained Q^2_{VDB} evolution as a function of the learning sample size (N_{LDB}) for a) γ-exponential GPM with 2 input parameters and b) Exponential GPM with 3 input parameters. It is observed that in the case when three input parameters ($1/T_{V/A}$, $a_{max\,out}$ and I_A) are adopted the variation of the estimated median Q^2_{VDB} value with N_{LDB} is very small.

Concerning the variance of the GPM, Figure 6(a) displays the obtained mean squared error (MSE) of predictions as a function of $1/T_{V/A}$ and $a_{max\,out}$ using the model with 3 input parameters. It is noted that the obtained MSE values are in general less than 0.2 for the cases when $a_{max\,out} < 1$g. On the other hand, it is important to note that for the same input values, a reduction in the MSE values is found with respect to the ones obtained when the GPM with 2 input parameters is used (Figure 6(b)). This figure shows the ratio between the MSE for 3 input parameters and the one for 2 input parameters (δMSE=MSE$_{3pr}$/MSE$_{2pr}$).

Finally, the GPM with 2 input parameters and with 3 input ones that provided the best fits are now used to simulate other earthquake scenarios (i.e. TDB with 445 signals). The mean $\delta u_{z,rel}/H$ values predicted by the two GPM are shown in Figure 7. It can be noted that both GP models selected for this study show a reasonable capability to reproduce the variation of $\delta u_{z,rel}/H$ as a function of $a_{max\,out}$. However, visually a less dispersion in the predicted values seems to be obtained using the 2 input parameters model for $a_{max\,out}$ values between 0.4 and 0.6g.

EVALUATION OF LEVEE VULNERABILITY USING GPM

In the context of the PBEE, the damage analysis, which is the third stage of this methodology, is a procedure to quantify the structural damage. It consists of setting fragility functions in order to find the conditional probability of the design to exceed a certain level of performance for a given seismic input motion parameter. Usually, fragility curves are constructed by using a single parameter to relate the level of shaking to the expected damage (Koutsourelakis et al. 2002; Baker and Cornell 2008a; Zentner 2010). So as to derive analytical fragility functions, it is necessary to define damage states in terms of some mechanical parameters that can be directly obtained from the analysis (e.g. $\delta u_{z,rel}/H$). The damage states limits or the performance levels of the levee are those proposed by Swaisgood (2003). The three damage levels thresholds are superposed in Figures 2(a) and 7. They correspond to $\delta u_{z,rel}/H$=0.02, 0.2 and 1.0%. In this work, the fragility curves are constructed following the methodology proposed by Shinozuka et al. (2000), i.e. the maximum likelihood method is used to compute numerical values of the estimators $\hat{\alpha}$ and $\hat{\beta}$ of Log-normal distribution.

The obtained fragility curves for the third and fourth state damages (i.e. minor to moderate and moderate to serious damages) are shown in Figure 8. These curves are drawn as solid lines whereas the statistical confidence of the derived fragility curves are drawn as dashed lines (i.e. $\{\hat{\alpha}\,\hat{\beta}\} \pm \{\sigma_1\,\sigma_2\}$). This confidence is a function of the information provided by the size of motion database over the parameters $\hat{\alpha}$ and $\hat{\beta}$ describing the shape of each curve and it is computed via the Fisher information matrix (Saez et al. 2011). Figure 8(a) presents fitted fragility functions obtained for two damage levels with respect to $a_{max\,out}$ using the FEM and the training dataset (LDB) (Figure 2(a)). These curves are used as reference case study. The obtained $\hat{\alpha}$, $\hat{\beta}$, σ_1 and σ_2 values at which the levee reaches the threshold of the minor to moderate and moderate to serious damages are provided in Table 3. According to Figure 8(a), it is clear that, for this database size, no enough information is available to develop a fragility curve for moderate to serious damages. It includes less information regarding statistical confidence of parameters. For a given value of $a_{max\,out}$, the probability of exceeding the damage threshold varies up to $\pm$ 15%. Consequently, a database including

a great number of ground motions is required to provide enough information to estimate in a reliable way the parameters defining the fragility curve (Luco and Cornell 2007; Seyedi et al. 2010; Lancieri et al. 2015). Due to the high computational cost to perform the numerous non-linear dynamic calculations of the TDB set with the FEM (Figure 1(c)), the proposed GPM with 3 input parameters was used. A comparison of the fragility curves obtained using the GPM and the FEM is displayed in Figure 8(b) and 8(c). This comparison is done for two damage levels (i.e. minor to moderate and moderate to serious damages) with respect to $a_{max\ out}$. GPM curves displayed in these figures have been derived using 445 ground motions (i.e. VDB and TDB set).

According to this comparison, the benefit of using a surrogate model appears principally in the reduction of the statistical confidence of the derived fragility curves for both damage levels by increasing the size of tested motions (i.e. the obtained σ_1 and σ_2 values, Table 3). It is noted that a reduction in the σ values for each fragility curve is obtained when the GPM predictions are used. A reduction of 70% for the case of minor to moderate damage and 50% for the moderate to serious damage. However, concerning the mean values, for the case of minor to moderate damage (Figure 8(b)), both $\hat{\alpha}$ and $\hat{\beta}$ estimators have similar values independent of the used database. On the contrary, for the moderate to serious damage (Figure 8(c)), it is noted that the fragility curve shifts slightly to higher acceleration values when the GPM is used. It means that for the same $a_{max\ out}$ input value a lower probability of exceedance is found. Finally, it is important to note that both curves obtained with the GPM are placed inside the statistical confidence of the derived FEM fragility curves. This parametric study confirms that the use of a well constructed surrogate models allows to obtain fragility curves with a reasonable accuracy and with a manageable computational effort.

Moreover, so as to assess the performance of the obtained GPM, a comparison between the computed fragility curves using the predicted values from the GPM and the obtained ones with FEM employing the TDB set is performed (Figure 9). It is noted that the curves

obtained using the two approaches are comparable. For the case of minor to moderate damage level (Figure 9(a)), some differences for higher acceleration values are remarked and on the contrary, for the moderate to serious damage level case the discrepancies are found for lower acceleration values (Figure 9(b)). These results confirm that for this particular case, the mean predicted GP values provide a good approximation to the FE outputs. However, it is clear that those differences could be reduced if the LDB is enriched with more input data in the regions where the variance is maximum (see Figure 6(a)).

Coming back to Figure 2(b), the response of the levee is a function of $a_{max\,out}$ and $1/T_{V/A}$, thus, the induced damage must be also related with a vector composed by various input motion parameters, characterizing different aspects of the shaking (Baker and Cornell 2008b; Seyedi et al. 2010). Hence, a comparison of the obtained distribution of the induced damage levels in the levee as two dimensional failure surfaces is provided in Figure 10. Figures 10(a) and 10(b) show the distribution obtained with the FEM using the LDB and with the GPM using the TDB respectively. It is remarked that the boundaries between each damage level are well defined for both studied cases and only few responses (i.e. a vector of $1/T_{V/A}$, $a_{max\,out}$ and DL) are overlapped. It is also noted the shape similarity between the observed surface (FEM-LDB) and the predicted one (GPM-TDB), which confirms again the applicability of the proposed metamodel to approximate the induced settlement and damage level in the levee for the range of parameters considered. Again from Figure 10, those results imply that instead of use fragility curves, fragility surfaces must be used to improve the representation of the strong ground motion in the damage assessment of the studied non-linear system (Seyedi et al. 2010). Nevertheless, this aspect is out of the scope of the present work but further researches will be done in this direction.

CONCLUSIONS

A FE analysis and a meta-model were used to investigate the soil liquefaction induced settlement and associated damage for an levee due to real earthquakes. Fragility functions were obtained for that purpose. The main conclusions drawn from this study are as follows:

Seismic demand fragility evaluation is one of the basic elements in the framework of performance-based earthquake engineering (PBEE). For solving the absence of sufficient Finite Element responses to obtain fragility curves with a reasonable accuracy, a Gaussian process model was build to mimic the FEM and used to increase the number of levee model evaluations reducing the computational time.

The predictive capability of the adopted GPM was assessed comparing the obtained levee settlements and induced damage levels with the ones simulated with the FEM. With respect to the case study considered, the GPM has shown a good capability of approximating the non-linear FEM response.

Results reveal that a GPM with three inputs parameters (i.e. $1/T_{V/A}$, $a_{max\,out}$ and I_A) to describe the liquefaction induced settlement of a levee, provides the most accurate estimates. Further investigations in this direction will be needed in order to obtain more general conclusions for diverse structure and soil typologies.

Based on these analyses, it is concluded that the proposed Gaussian process model is accurate enough for practical purposes and represents an important economy in CPU consumption time. It is confirmed by the comparison between the fragility curves obtained by the two methods on the test data set.

Further research can be done to ameliorate the results as to account for a better way to select the input parameters and to minimize the number of FEM computations so as to reduce discrepancies between both models (i.e. FEM and GPM).

Finally, it was found that fragility surfaces must be used to improve the representation of the strong ground motion in the damage assessment of the studied non-linear system. Further researches will be done in this direction.

ACKNOWLEDGEMENTS

This work, within the SINAPS@ project, benefited from French state funding managed by the National Research Agency under program RNSR Future Investments bearing reference No. ANR-11-RSNR-0022-04. The research reported in this paper has been supported in

part by the SEISM Paris Saclay Research Institute.

The authors acknowledge accessing strong-motion data through the Center for Engineering Strong Motion Data (CESMD), last visited on Aug 2017. The networks or agencies providing the data used in this report are the California Strong Motion Instrumentation Program (CSMIP) and the USGS National Strong Motion Project (NSMP).

REFERENCES

Ancheta, T. D., Darragh, R. B., Stewart, J. P., Seyhan, E., Silva, W. J., Chiou, B. S. J., Wooddell, K. E., Graves, R. W., Kottke, A. R., Boore, D. M., Kishida, T., and Donahue, J. L. (2013) PEER NGA-W*est2* D*atabase*. PEER Report No. 2013/03, Pacific Earthquake Engineering Research Center, University of California, Berkeley, CA.

Aoi, S., Obara, K., Hori, S., Kasahara, K., and Okada, Y. (2001). "New Japanese uphole-downhole strong-motion observation network: KiK-net." *Seismological Research Letters*, 72:239.

Aubry, D., Chouvet, D., Modaressi, A., and Modaressi, H. (1986). "GEFD*yn*: Logiciel d'Analyse de Comportement Mécanique des Sols par Eléments Finis avec Prise en Compte du Couplage Sol-Eau-Air." *Manuel scientifique*, Ecole Centrale Paris, LMSS-Mat.

Aubry, D., Hujeux, J.-C., Lassoudière, F., and Meimon, Y. (1982). "A double memory model with multiple mechanisms for cyclic soil behaviour." *International symposium on numerical models in geomechanics*, Balkema, 3–13.

Aubry, D. and Modaressi, A. (1996). "GEFD*yn*." *Manuel scientifique*, Ecole Centrale Paris, LMSS-Mat.

Baker, J. W. and Cornell, C. A. (2008a). "Uncertainty propagation in probabilistic seismic loss estimation." *Structural Safety*, 30(3), 236–252.

Baker, J. W. and Cornell, C. A. (2008b). "Vector-valued Intensity Measures Incorporating Spectral Shape For Prediction of Structural Response." *Journal of Earthquake Engineering*, 12(4), 534–554.

Bucher, C. and Most, T. (2008). "A comparison of approximate response functions in structural reliability analysis." *Probabilistic Engineering Mechanics*, 23(2-3), 154 – 163.

Byrne, P. M., Park, S.-S., Beaty, M., Sharp, M., Gonzalez, L., and Abdoun, T. (2004). "Numerical

modeling of liquefaction and comparison with centrifuge tests." *Canadian Geotechnical Journal*, 41(2), 193–211.

Cardoso, J. B., de Almeida, J. R., Dias, J. M., and Coelho, P. G. (2008). "Structural reliability analysis using monte carlo simulation and neural networks." *Advances in Engineering Software*, 39(6), 505 – 513.

DiazDelaO, F. A., Adhikari, S., Saavedra Flores, E. I., and Friswell, M. I. (2013). "Stochastic structural dynamic analysis using bayesian emulators." *Computers & Structures*, 120(1), 24 – 32.

Dubourg, V., Sudret, B., and Deheeger, F. (2013). "Metamodel-based importance sampling for structural reliability analysis." *Probabilistic Engineering Mechanics*, 33, 47–57.

Ferrario, E., Pedroni, N., Zio, E., and Lopez-Caballero, F. (2017). "Bootstrapped Artificial Neural Networks for the seismic analysis of structural systems." *Structural Safety*, in-press.

Genton, M. G. (2001). "Classes of kernels for machine learning: a statistics perspective." *Journal of Machine Learning Research*, 2(1), 299 – 312.

Ghosh, J., Padgett, J. E., and Dueñas-Osorio, L. (2013). "Surrogate modeling and failure surface visualization for efficient seismic vulnerability assessment of highway bridges." *Probabilistic Engineering Mechanics*, 34(1), 189 – 199.

Gidaris, I., Taflanidis, A. A., and Mavroeidis, G. P. (2015). "Kriging metamodeling in seismic risk assessment based on stochastic ground motion models." *Earthquake Engineering & Structural Dynamics*, 44(14), 2377–2399.

Iooss, B., Boussouf, L., Feuillard, V., and Marrel, A. (2010). "Numerical studies of the metamodel fitting and validation processes." *International Journal On Advances in Systems and Measurements, IARIA*, 3, 11–21.

Juang, C. H., Yuan, H., Li, D. K., Yang, S. H., and Christopher, R. A. (2005). "Estimating severity of liquefaction-induced damage near foundation." *Soil Dynamics and Earthquake Engineering*, 25(5), 403–411.

Kawase, H. (2011). "Strong motion characteristics and their damage impact to structures during the Off Pacific Coast of Tohoku earthquake of march 11, 2011; How extraordinary was this M9.0 earthquake?." *4th IASPEI / IAEE International Symposium: Effects of Surface Geology*

on Seismic Motion, University of California Santa Barbara.

Kayen, R. E. and Mitchell, J. K. (1997). "Assessment of liquefaction potential during earthquakes by arias intensity." *Journal of Geotechnical and Geoenvironmental Engineering*, 123(12), 1162–1175.

Koutsourelakis, S., Prévost, J. H., and Deodatis, G. (2002). "Risk assessment of an interacting structure-soil system due to liquefaction." *Earthquake Engineering and Structural Dynamics*, 31(4), 851–879.

Lancieri, M., Renault, M., Berge-Thierry, C., Gueguen, P., Baumont, D., and Perrault, M. (2015). "Strategy for the selection of input ground motion for inelastic structural response analysis based on naïve bayesian classifier." *Bulletin of Earthquake Engineering*, 13(9), 2517–2546.

Lopez-Caballero, F. and Modaressi-Farahmand-Razavi, A. (2008). "Numerical simulation of liquefaction effects on seismic SSI." *Soil Dynamics and Earthquake Engineering*, 28(2), 85–98.

Lopez-Caballero, F. and Modaressi-Farahmand-Razavi, A. (2010). "Assessment of variability and uncertainties effects on the seismic response of a liquefiable soil profile." *Soil Dynamics and Earthquake Engineering*, 30(7), 600–613.

Luco, N. and Cornell, C. A. (2007). "Structure-Specific Scalar Intensity Measures for Near-Source and Ordinary Earthquake Ground Motions." *Earthquake Spectra*, 23(2), 357–392.

Matsuo, O. (1996). "Damage to river dikes." *Soils and Foundations*, 36(1), 235–240.

Modaressi, H. and Benzenati, I. (1994). "Paraxial approximation for poroelastic media." *Soil Dynamics and Earthquake Engineering*, 13(2), 117–129.

National Academies of Sciences, Engineering, and Medicine (2016). *State of the Art and Practice in the Assessment of Earthquake-Induced Soil Liquefaction and Its Consequences*. The National Academies Press, Washington, DC.

Oka, F., Tsai, P., Kimoto, S., and Kato, R. (2012). "Damage patterns of river embankments due to the 2011 off the pacific coast of tohoku earthquake and a numerical modeling of the deformation of river embankments with a clayey subsoil layer." *Soils and Foundations*, 52(5), 890–909.

Okamura, M., Tamamura, S., and Yamamoto, R. (2013). "Seismic stability of embankments subjected to pre-deformation due to foundation consolidation." *Soils and Foundations*, 53(1), 11 – 22.

Ozutsumi, O., Sawada, S., Iai, S., Takeshima, Y., Sugiyama, W., and Shimazu, T. (2002). "Effective stress analyses of liquefaction-induced deformation in river dikes." *Soil Dynamics and Earthquake Engineering*, 22(9-12), 1075 – 1082.

Popescu, R., Prévost, J. H., Deodatis, G., and Chakrabortty, P. (2006). "Dynamics of nonlinear porous media with applications to soil liquefaction." *Soil Dynamics and Earthquake Engineering*, 26(6-7), 648–665.

Porter, K. A. (2003). "An overview of PEER's Performance-Based Earthquake Engineering Methodology." *Ninth International Conference on Applications of Statistics and Probability in Civil Engineering (ICASP9) July 6-9, San Francisco*.

Rapti, I., Lopez-Caballero, F., Modaressi-Farahmand-Razavi, A., Foucault, A., and Voldoire, F. (2017). "Liquefaction analysis and damage evaluation of embankment-type structures." *Acta Geotechnica*, in-press.

Rasmussen, C. E. and Williams, C. K. I. (2006). *Gaussian Processes for Machine Learning*. the MIT Press.

Roustant, O., Ginsbourger, D., and Deville, Y. (2012). "DiceKriging, DiceOptim: Two R packages for the analysis of computer experiments by kriging-based metamodeling and optimization." *Journal of Statistical Software*, 51(1), 1–55.

Sacks, J., Welch, W. J., Mitchell, T. J., and Wynn, H. P. (1989). "Design and analysis of computer experiments." *Statistical Science*, 4(4), 409–423.

Saez, E., Lopez-Caballero, F., and Modaressi-Farahmand-Razavi, A. (2011). "Effect of the inelastic dynamic soil-structure interaction on the seismic vulnerability assessment." *Structural Safety*, 33(1), 51–63.

Seed, H. B. and Idriss, I. M. (1971). "Simplified procedure for evaluating soil liquefaction potential." *Journal of Soil Mechanics and Foundations Division - ASCE*, 97(SM9), 1249–1273.

Seo, J., Dueñas-Osorio, L., Craig, J. I., and Goodno, B. J. (2012). "Metamodel-based regional vulnerability estimate of irregular steel moment-frame structures subjected to earthquake events." *Engineering Structures*, 45(1), 585 – 597.

Seyedi, D. M., Gehl, P., Douglas, J., Davenne, L., Mezher, N., and Ghavamian, S. (2010). "Development of seismic fragility surfaces for reinforced concrete buildings by means of nonlinear

time-history analysis." *Earthquake Engineering & Structural Dynamics*, 39(1), 91–108.

Sharp, M. K. and Adalier, K. (2006). "Seismic response of earth dam with varying depth of liquefiable foundation layer." *Soil Dynamics and Earthquake Engineering*, 26(11), 1028–1037.

Shinozuka, M., Feng, Q., Lee, J., and Naganuma, T. (2000). "Statistical analysis of fragility curves." *Journal of Engineering Mechanics - ASCE*, 126(12), 1224–1231.

Stern, R., Song, J., and Work, D. (2017). "Accelerated Monte Carlo system reliability analysis through machine-learning-based surrogate models of network connectivity." *Reliability Engineering & System Safety*, 164(1), 1–9.

Strong, M. and Oakley, J. E. (2014). "When is a model good enough? deriving the expected value of model improvement via specifying internal model discrepancies." *SIAM/ASA Journal on Uncertainty Quantification*, 2(1), 106–125.

Swaisgood, J. R. (2003). "Embankment dam deformation caused by earthquakes." *Pacific Conference on Earthquake Engineering*, Paper no. 014.

Toal, D. J. J., Bressloff, N. W., and Keane, A. J. (2008). "Kriging Hyperparameter Tuning Strategies." *AIAA Journal*, 46(5), 1240–1252.

Unjoh, S., Kaneko, M., Kataoka, S., Nagaya, K., and Matsuoka, K. (2012). "Effect of earthquake ground motions on soil liquefaction." *Soils and Foundations*, 52(5), 830–841.

Zentner, I. (2010). "Numerical computation of fragility curves for NPP equipment." *Nuclear Engineering and Design*, 240(6), 1614 – 1621.

Zienkiewicz, O. C. and Shiomi, T. (1984). "Dynamic behaviour of saturated porous media; the generalised biot formulation and its numerical solution." *International Journal for Numerical and Analytical Methods in Geomechanics*, 8, 71–96.

List of Tables

TABLE 1. Statistics characteristics for the selected earthquakes in each database (DB)

Parameter	LDB Range	VDB Range	TDB Range
$a_{max\,out}$ [g]	$0.01 - 1.93$	$0.03 - 1.16$	$0.03 - 1.93$
T_m [s]	$0.12 - 1.69$	$0.17 - 1.69$	$0.17 - 1.81$
$T_{V/A}$ [s]	$0.09 - 1.91$	$0.13 - 1.42$	$0.13 - 1.32$
I_A [m/s]	$0.001 - 20.64$	$0.04 - 4.13$	$0.004 - 20.64$
D_{5-95} [s]	$2.26 - 69.84$	$2.96 - 42.77$	$2.26 - 47.36$
PGV [cm/s]	$0.23 - 167.6$	$4.27 - 83.58$	$0.86 - 166.1$
DB Size	95	50	395

TABLE 2. Relative error between the GPM predictions and the FEM computations. Case of VDB set.

Covariance Function	Q^2_{VDB} [1] 2 input param. N_{LDB}=95	Q^2_{VDB} [1] 3 input param. N_{LDB}=95
Matérn (3/2)	0.63	0.83
Exponential	0.74	0.94
γ-exponential ($\gamma = 2$)	0.80	0.93

TABLE 3. Fragility curve parameters from the mean GPM predictions (TDB set) and the FEM computations (LDB set).

Damage	FEM				GPM				$\sigma_{\mathrm{GPM}}/\sigma_{\mathrm{FEM}}$	
state	$\hat{\alpha}$	$\hat{\beta}$	σ_1	σ_2	$\hat{\alpha}$	$\hat{\beta}$	σ_1	σ_2	σ_1	σ_2
DL III	0.21	0.26	0.015	0.067	0.21	0.21	0.005	0.023	0.33	0.34
DL IV	0.45	0.51	0.041	0.135	0.47	0.53	0.021	0.068	0.51	0.50

List of Figures

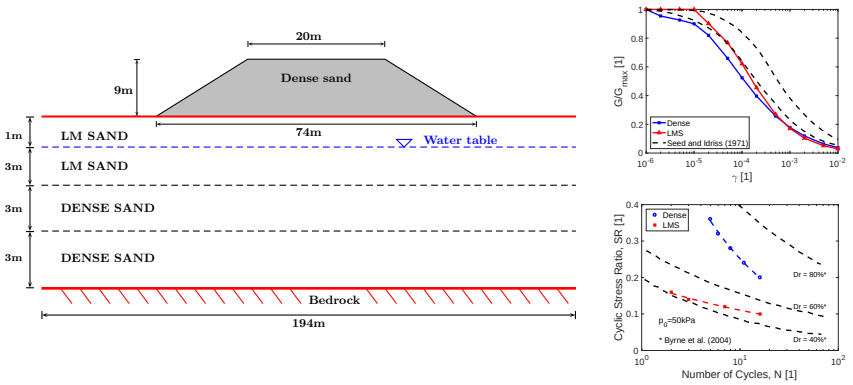

(a)

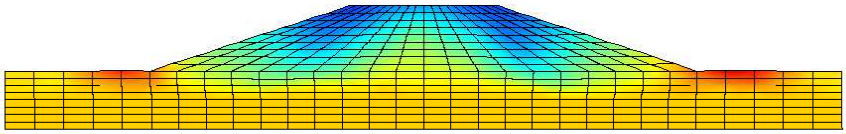

Vertical Displacement [m]

-0.2 -0.1 0 0.1

(b)

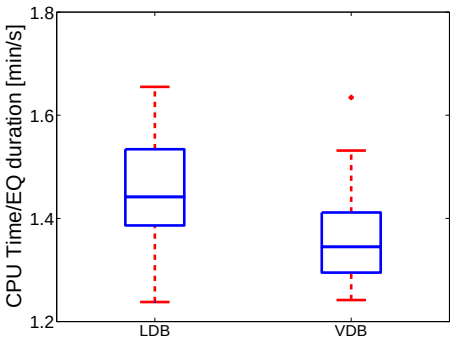

(c)

FIG. 1. a) Geometry and behaviour of soils used in the numerical model; b) Enlarged view of typical vertical co-seismic displacement contours at the end of the shaking and c) box plot of the ratio of CPU time per earthquake duration spent to perform the computations using LDB and VDB sets.

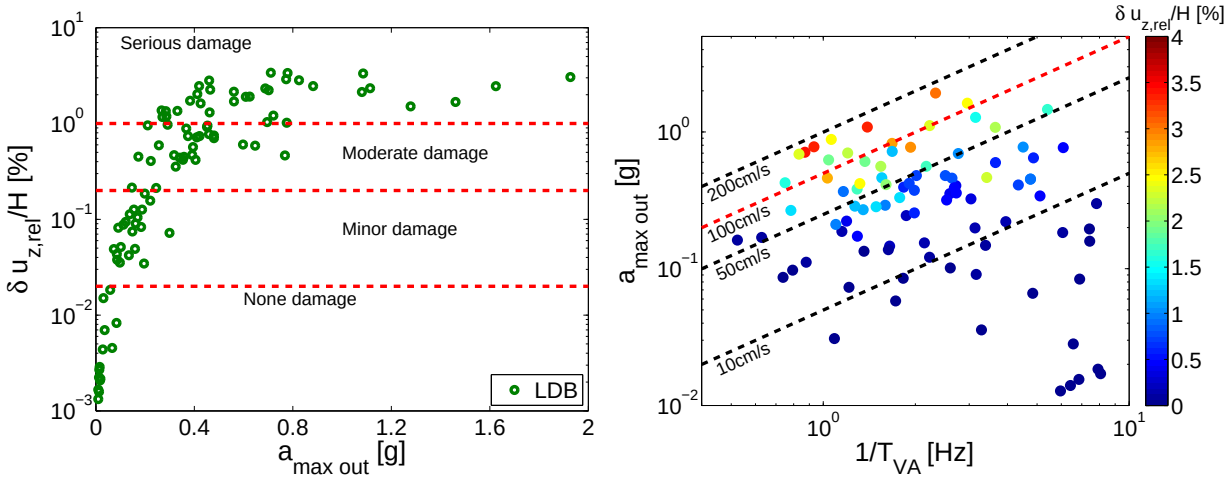

(a) (b)

FIG. 2. Scatter plot of crest settlement ratio of the FE model as a function of a) $a_{max\,out}$ **and b)** $a_{max\,out}$ **and** $1/T_{V/A}$**. Case of LDB sets.**

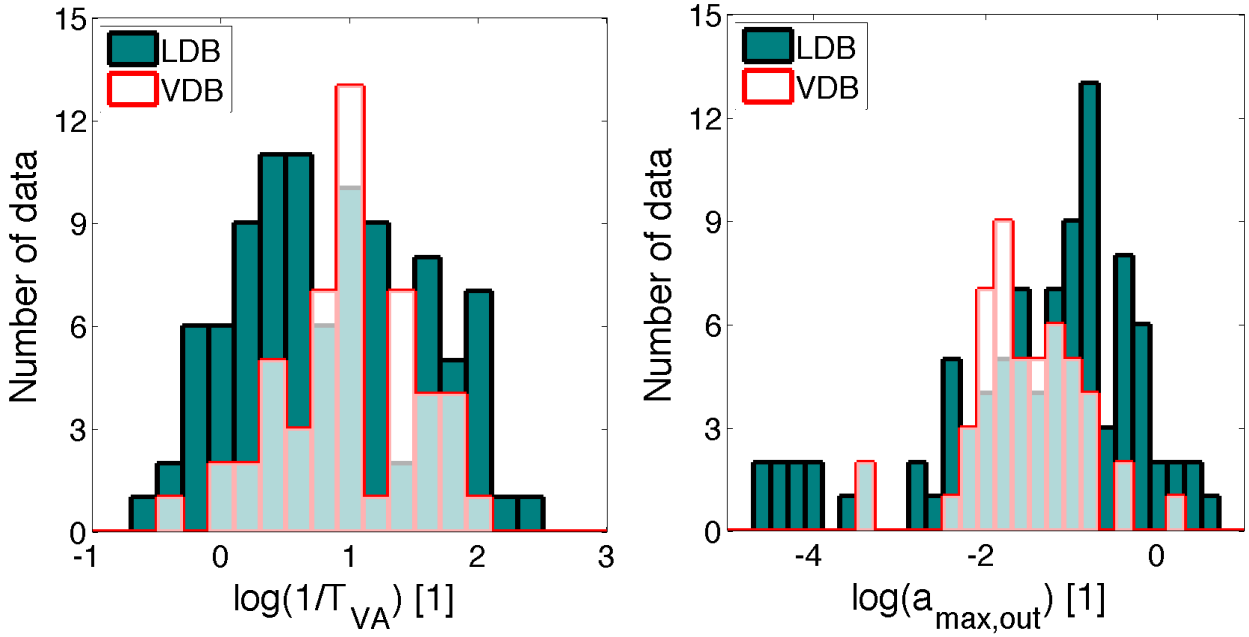

(a) (b)

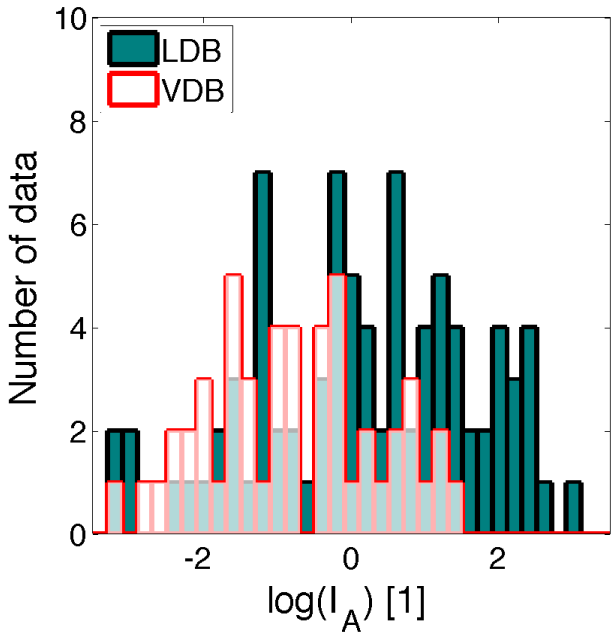

(c)

FIG. 3. Comparison of the distribution of the GPM input parameters for LDB and VDB; a) $1/T_{V/A}$**; b)** $a_{max\,out}$ **and c)** I_A**.**

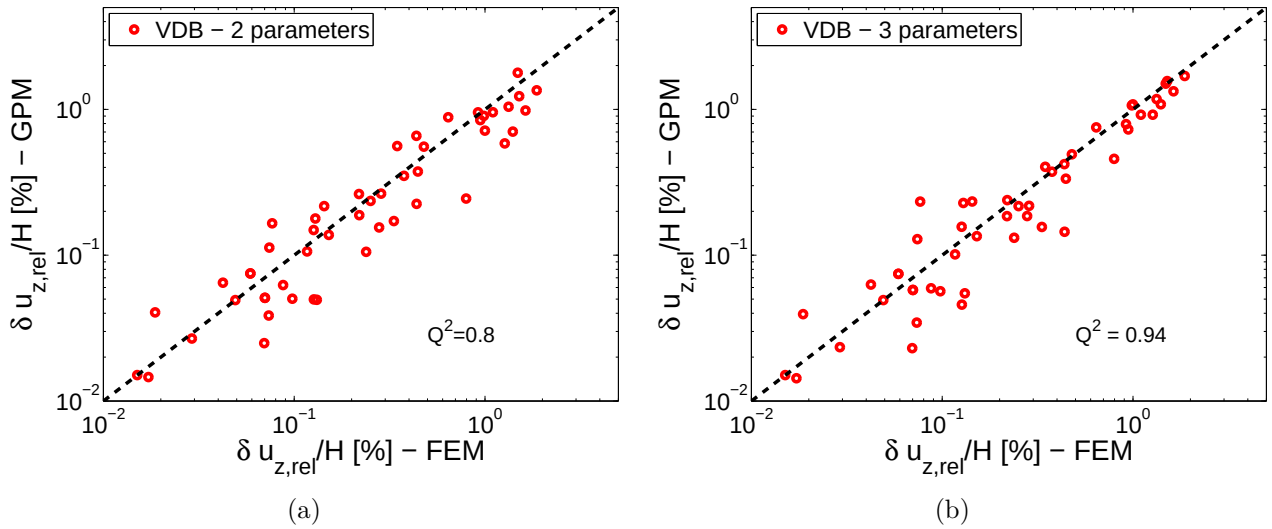

FIG. 4. Comparison of $\delta u_{z,rel}/H$ values obtained with FEM and with GPM approaches. a) γ-exponential GPM with 2 input parameters and b) Exponential GPM with 3 input parameters. Case of VDB sets.

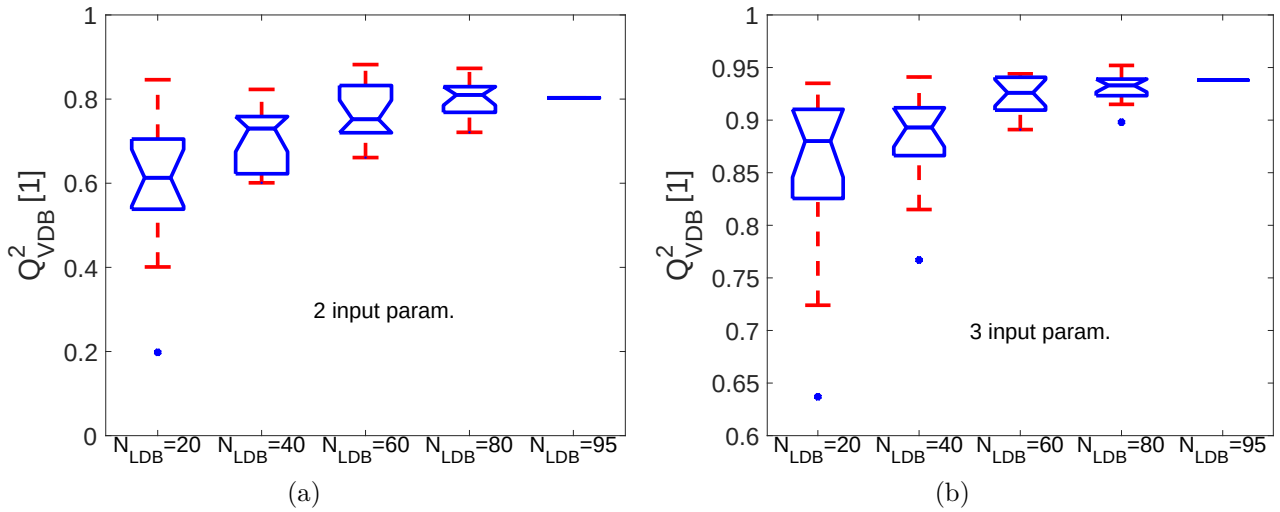

FIG. 5. Estimated Q^2_{VDB} evolution as a function of the learning sample size (N_{LDB}) for a) γ-exponential GPM with 2 input parameters and b) Exponential GPM with 3 input parameters. Case of VDB sets.

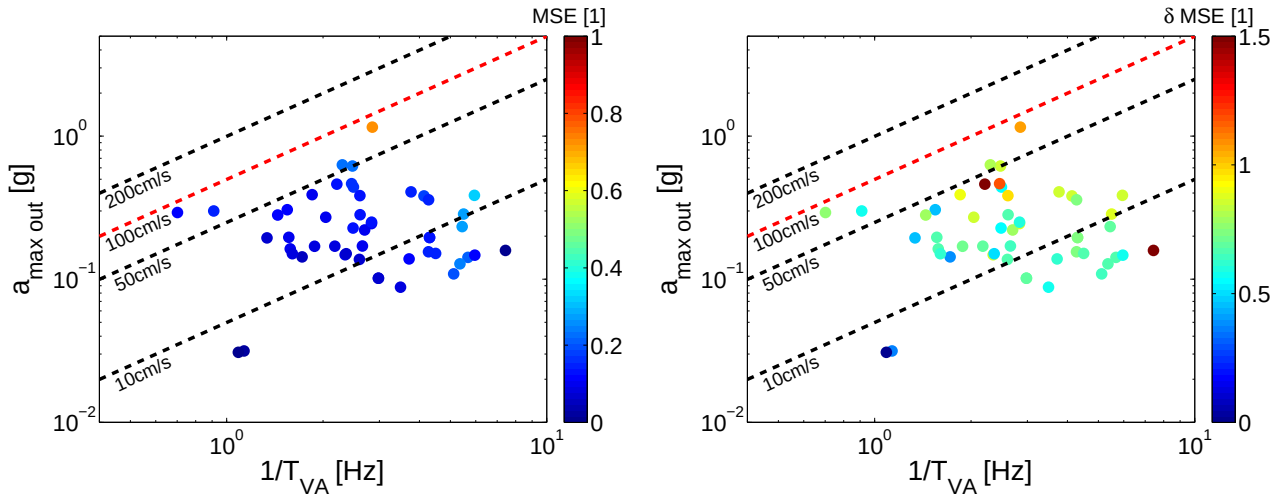

FIG. 6. a) Obtained mean squared error (MSE) in the prediction of $\delta u_{z,rel}/H$ values obtained using GPM with 3 input parameters and b) Ratio between the obtained MSE for 3 input parameters and the MSE for 2 input parameters (δMSE=MSE$_{3pr}$/MSE$_{2pr}$). Case of VDB sets.

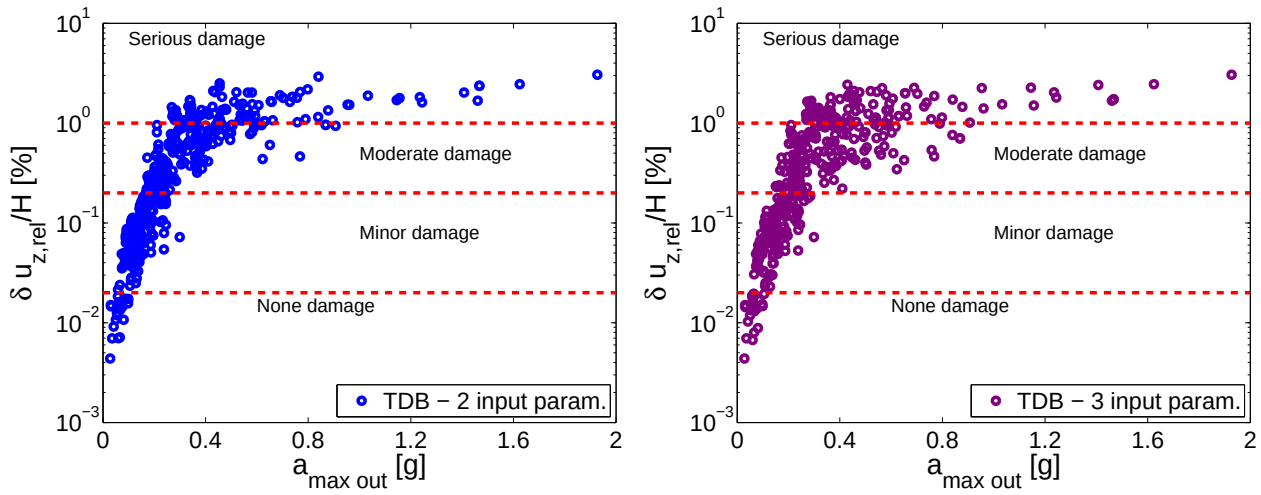

(a) (b)

FIG. 7. Mean predicted $\delta u_{z,rel}/H$ as a function of $a_{max\,out}$ obtained with the GPM approach. a) GPM with 2 input parameters and b) GPM with 3 input parameters. Case of TDB sets.

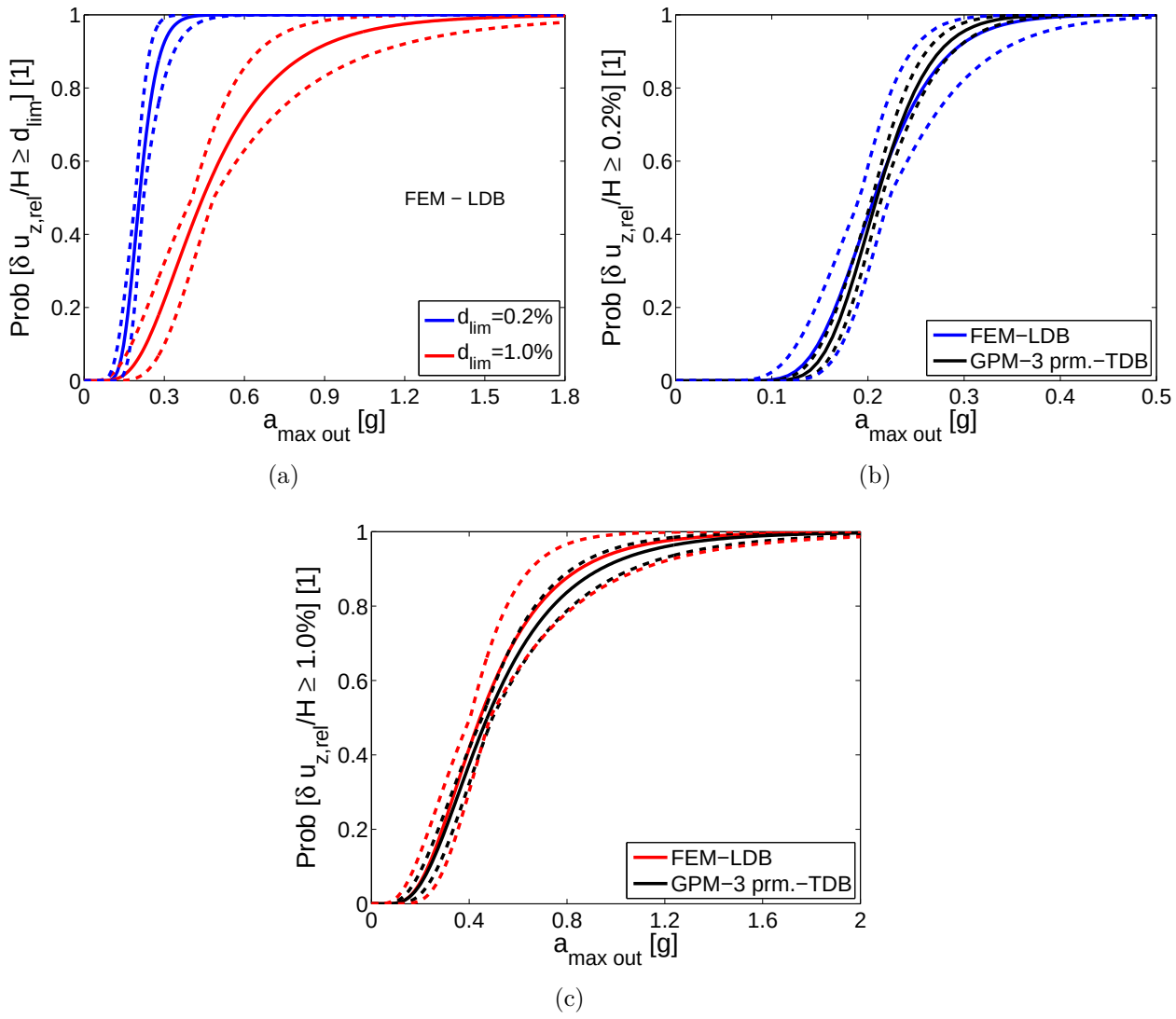

FIG. 8. Computed fragility curves for two damage levels following a) FEM approach; b) and c) FEM and GPM approaches.

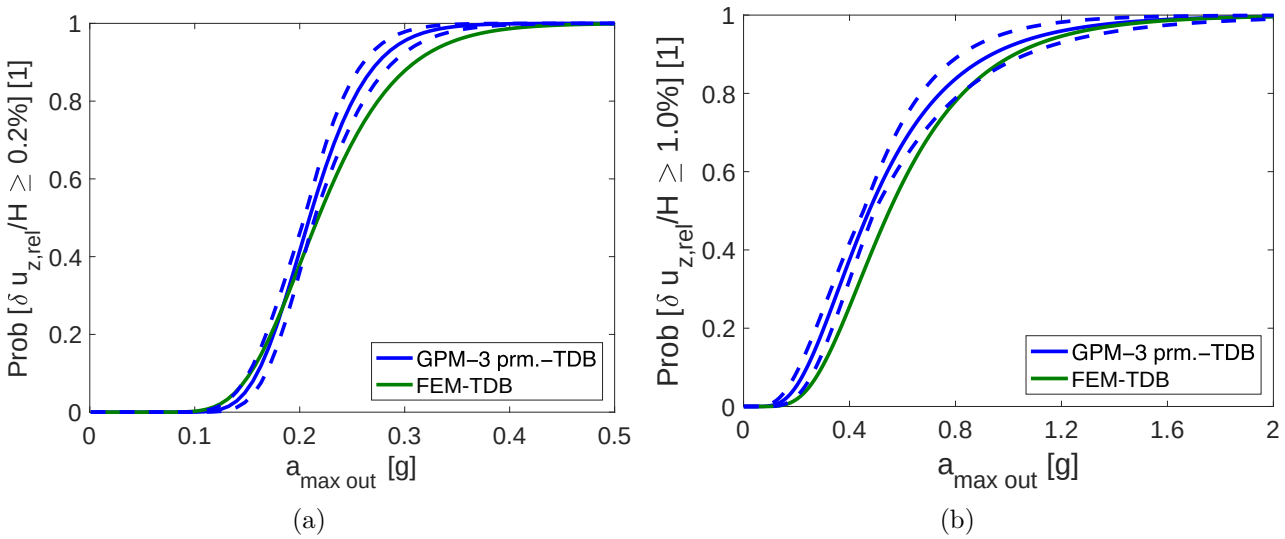

(a) (b)

FIG. 9. Computed fragility curves for two damage levels, a) minor to moderate and b) moderate to serious damages. Comparison of responses obtained with FEM and predicted with GPM using the TDB sets.

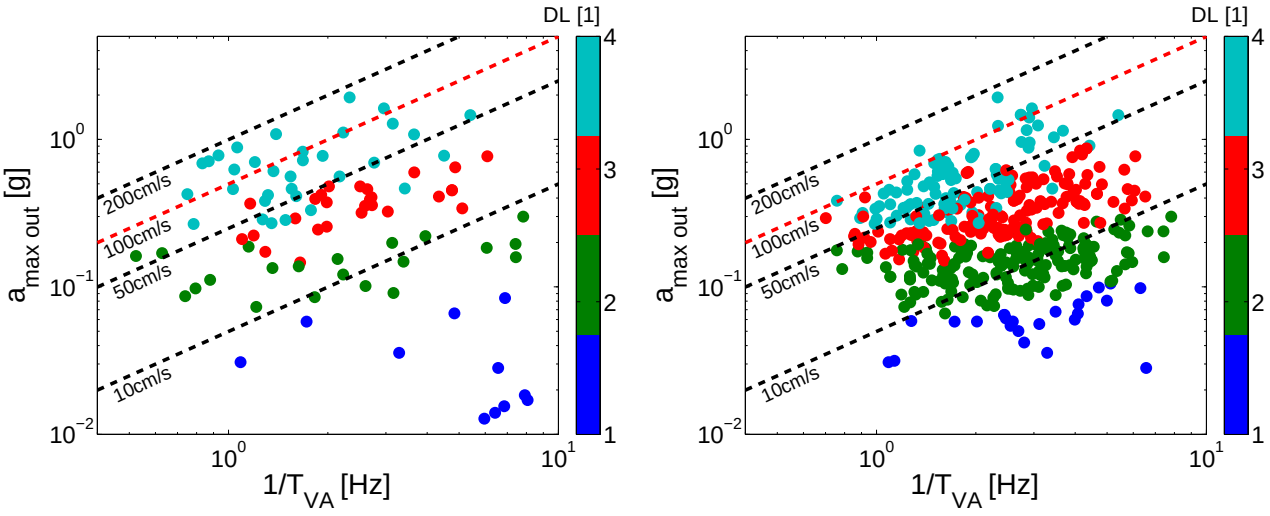

FIG. 10. Two dimensional failure surface, a) FEM with LDB set and b) GPM with TDB set.